RSC Advances

COMMUNICATION

View Article Online
View Journal | View Issue

Cite this: *RSC Adv.*, 2014, **4**, 36682

Received 24th May 2014
Accepted 4th August 2014

DOI: 10.1039/c4ra04922e

www.rsc.org/advances

Internal and external morphology-dependent plasmonic resonance in monolithic nanoporous gold nanoparticles†

Jianbo Zeng,[a] Fusheng Zhao,[a] Ji Qi,[a] Yifei Li,[a] Chien-Hung Li,[b] Yan Yao,[ac] T. Randall Lee[bc] and Wei-Chuan Shih*[ad]

We report morphology-dependent plasmonic resonance in monolithic nanoporous gold nanoparticles with a nanoscale internal porous network produced by the combination of lithographic patterning and dealloying. Timed dealloying and post-dealloying thermal annealing techniques have been employed to precisely control the morphological evolution. We found that prolonged dealloying time caused further pore coarsening to increase by ~4 nm, whereas thermal annealing induced both pore coalescence and disk shrinkage, which eventually led to pore elimination. Both types of morphological changes caused a blueshift in the major plasmonic extinction band of up to 200 nm, in contrast to the redshift (~50 nm) observed in semi-infinite NPG thin films. In addition, a greater blueshift was observed in a higher Au atomic content starting alloy. The tunable plasmonic properties have great potential in surface-enhanced spectroscopy and optical sensing.

Introduction

Semi-infinite nanoporous gold (NPG) films feature nanoscale ligaments and pore channels within their unique bicontinuous porous nanostructures with associated interesting plasmonic properties.[1–3] The enhanced electromagnetic (EM) fields of *localized surface plasmon resonance* (LSPR) excited in the ligaments are considered to be a major contributor to LSPR sensing and surface-enhanced optical phenomena such as surface-enhanced Raman scattering (SERS) and surface-enhanced fluorescence.[4–6] Limited tunability in plasmonic resonance can be achieved by varying the morphology of porous nanostructures such as the pore and ligament size through dealloying time and thermal annealing.[3,7,8] Specifically, spectral redshift has been observed in NPG thin films obtained by prolonged dealloying or thermal annealing, where emphasis has been put on mechanical properties, thermal conductivity, and application in SERS.[8–10]

Unlike semi-infinite NPG films, recent demonstration of patterned monolithic NPG nanoparticles, featuring nanoscale pores and sub-micron disk shape, represent a new class of NPG material that inherits plasmonic features from both the nanoporous structures ("NPG LSPR") and the sub-wavelength disk shape ("Disk LSPR").[11,12] The large surface area of NPG nanoparticles and hot-spots inside the nanoporous structures have contributed to an average SERS enhancement factor exceeding 10^8 and surprisingly high photothermal conversion efficiency (~56%) among metal nanoparticles of similar size with various shapes and compositions such as nanoshells (~30%) and Cu_9S_5 nanocrystals (~25.7%).[12–15] NPG disk substrates have also been employed for biomolecular sensing by a novel stamping approach without any wet sample preparation and in microfluidics.[16,17] In addition, the coupling between disk shape and the nanopores has produced significant redshift in both of them compared to that for NPG films in the literature.[11] Further, both the pore size and disk size become critical parameters governing NPG disk plasmonic resonance, compared to only the pore size parameter for semi-infinite NPG films.

We are particularly interested in exploring the plasmonic tunability of monolithic NPG nanoparticles by timed dealloying and thermal annealing induced *external and internal* morphological changes. Specifically, increased dealloying time results in internal morphological evolution such as size growth of both the pore and ligament, thus further coarsening the porous network. Thermal annealing, in contrast, introduces both external morphological changes such as disk thickness and diameter reduction, as well as internal modifications such as pore coalescence. We show widely tunable plasmonic resonance is achievable in the spectral region from 700 to 1000 nm by

[a]*Department of Electrical and Computer Engineering, University of Houston, 4800 Calhoun Road, Houston, TX 77204, USA. E-mail: wshih@uh.edu; Fax: +1-713-743-4444; Tel: +1-713-743-4454*

[b]*Department of Chemistry, University of Houston, 4800 Calhoun Road, Houston, TX 77204, USA*

[c]*Texas Center for Superconductivity, University of Houston, 4800 Calhoun Road, Houston, TX 77204, USA*

[d]*Department of Biomedical Engineering, University of Houston, 4800 Calhoun Road, Houston, TX 77204, USA*

† Electronic supplementary information (ESI) available: XPS analysis and SEM images of NPG disk thermal annealing. See DOI: 10.1039/c4ra04922e

these strategies. Specifically, blueshift of the major plasmonic extinction band has been observed due to morphological changes, in contrast to predominantly redshift as documented in the literature, thus providing new evidence to support our interpretation that the major plasmonic extinction band belongs to the in-plane resonance of the disk shape (*i.e.*, Disk LSPR), not the nanopores (*i.e.*, NPG LSPR).[11] It also supports that coupling exists between these two modes. Moreover, we show the plasmonic resonance can be tuned by varying the Au atomic composition in the starting alloy.

Materials and methods

Chemicals and materials

Ethanol (200 proof) was from Decon Laboratories, Inc. Nitric acid (ACS reagent, 70%), sodium dodecyl sulfate (ACS reagent, ≥99.0%), chloroform (anhydrous, ≥99.0%), and latex beads (polystyrene beads, 10% aqueous suspension) with mean particle sizes 460 nm were purchased from Sigma Aldrich. $Ag_{82.5}Au_{17.5}$ and $Ag_{70}Au_{30}$ (atomic percentage) alloy sputtering targets was purchased from ACI Alloys, Inc. Argon gas (99.999%) was used for RF-sputter etching and protection of thermal annealing. Fusion classic syringe pumps and microliter syringes (250 μl) were purchased from Chemyx Inc. and Hamilton Company, respectively. Silicon wafers were obtained from University Wafers, and coverglass (22 × 40 mm, No.1) from VWR.

Fabrication of monolithic NPG nanoparticles. Detailed fabrication process was described in elsewhere of our work.[11–13] Briefly, a self-assembled monolayer of 460 nm polystyrene (PS) beads on an alloy film covered glass substrate was prepared according to a previously reported procedure.[18,19] The 120 nm thick Au/Ag alloy film was deposited by sputtering using an alloy target. The Au/Ag alloy film covered with PS bead monolayer was first etched 2 min in oxygen plasma to shrink the PS beads at 30 mTorr and 100 W, and then the sample was further etched in a 2 mTorr/100 W Argon plasma for 12 min to obtain Au/Ag alloy nanoparticles. The remaining polystyrene was removed by sonication in chloroform for 1 min. Finally, the NPG nanoparticles were formed by dealloying Ag in 70% nitric acid varying from 30 to 270 s. The sample was washed in deionized (DI) water to remove the dealloying reaction products and excess nitric acid. The as-dealloyed NPG nanoparticles were subjected to thermal annealing within a programmed tube furnace at 100, 200, 300, 400, and 500 °C for 30 min with ambient Argon gas.

Characterization. A Cary 50 Scan UV-visible spectrometer was used to measure the UV-vis spectra from 300 to 1100 nm of the monolayer NPG nanoparticle samples measured ~1.0 mm × 0.5 mm. The samples were characterized by a scanning electron microscope (SEM) (PHILIPS FEI XL-30 FEG SEM). X-ray photoelectron spectroscopy (XPS) spectra were obtained using a PHI 5700 system equipped with a monochromatic Al Kα X-ray source ($h\nu$ = 1486.7 eV). High Pressure Tube Furnace OTF-1200X (MTI Corporation, USA) was used for thermal annealing. The Raman spectra of benzenethiol were recorded by using a home-built line-scan Raman microscope (LSRM) as described in our previous paper.[20]

Results and discussion

Dealloying time dependent blueshift

Scanning electron microscopy (SEM) images of samples obtained from $Ag_{82.5}Au_{17.5}$ after dealloying for 30, 150 and 270 s in concentrated nitric acid (HNO_3) are shown in Fig. 1a–c, respectively. For 30 s, the average pore size was about 11.7 nm (Fig. 1a), and the average ligament size was about 14.5 nm, where the size were measured at the minimum width of the pore and ligament. When the dealloying time was increased to 270 s (Fig. 1c), the average size of pores and ligaments increased to 15.5 and 21.3 nm, respectively. Fig. 1d summarized the growth trend of the pore and ligament size during the dealloying process from 30 to 270 s. At the initial stage, the rapid etching of Ag atoms and extremely fast surface diffusion of gold atoms at the alloy/nitric acid interface form small pores and ligaments within short time. Under further dealloying, the diffusive gold atoms tend to condense onto gold-rich clusters that results in the growth of the pore and ligament size.[21–23] Moreover, the statistical average thickness and diameter with different dealloying times were ~74 ± 2 and 300 ± 8 nm, respectively. Thus, there was no apparent change in the external dimension with respect to dealloying time.

Fig. 2a shows the atomic fraction of Au and Ag *versus* dealloying time and typical XPS spectra of Ag 3d and Au 4f are provided in Fig. S1.† The atomic fraction of Ag rapidly dropped within the first 30 s of dealloying because of the fast Ag leeching rate in concentrated nitric acid and plateaued after 90 s. However, pore coarsening continued after 90 s when the composition stayed relatively constant. Interestingly, further dealloying caused the Ag fraction to slightly increase, suggesting that Au began to depart after a longer dealloying time. A similar observation on Au loss has also been reported by Gupta

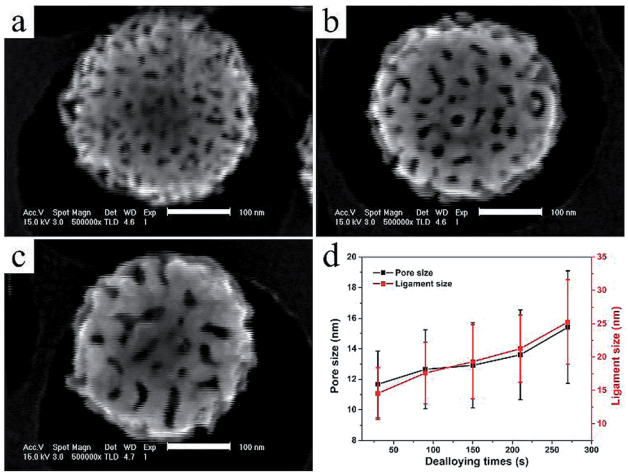

Fig. 1 SEM images and image analysis of 300 nm diameter NPG nanoparticles made from $Ag_{82.5}Au_{17.5}$ alloy for different dealloying time: (a) 30, (b) 150 and (c) 270 s. (d) pore and ligament sizes based on statistical analysis *versus* dealloying time. SEM scale bar: 100 nm.

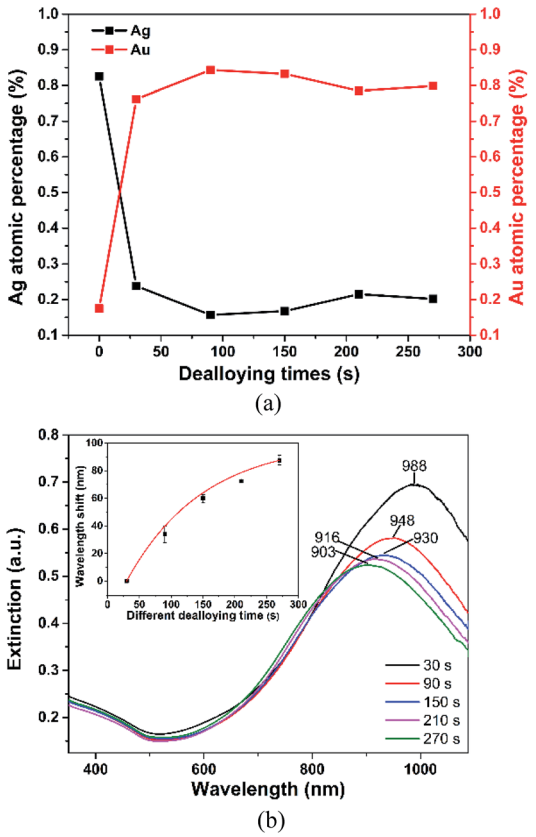

Fig. 2 Elemental composition and extinction spectra of 300 nm diameter NPG disk made from $Ag_{82.5}Au_{17.5}$ alloy: (a) atomic percentage of Ag and Au *versus* dealloying time. (b) extinction spectra *versus* dealloying time. The inset shows blueshift *versus* dealloying time. The curve is only for visual guidance.

and coworkers when investigating NPG films by Rutherford backscattering spectrometry.[24]

In Fig. 2b, NPG nanoparticles dealloyed for 30 s exhibited an extinction band at 988 nm, which has been interpreted as the in-plane resonance of the disk (*i.e.*, Disk LSPR), while the band around 600 nm assigned as NPG localized surface plasmonic resonance (*i.e.*, NPG LSPR) was not obvious due to peak broadening caused by random nanoporous structures and nanoscale Au ligaments.[11] We observed that the in-plane resonance band blueshifted ~40 nm as the dealloying time was increased to 90 s, and it further blueshifted with longer dealloying times. For 270 s dealloying, the blueshift was 85 nm. The inset shows the wavelength shift *versus* dealloying time and the error bars are the standard deviation of three different measurements. More significant blueshift has been observed for the first 90 s of dealloying.

Chen and coworkers investigated the plasmonic tunability of semi-infinite NPG films with respect to its pore sizes, and found that the band over 500 nm, assigned to NPG LSPR, redshifted as the pore sizes increased.[3] The increased ligament sizes resulting in the longer effective electron oscillation lengths and the redshift. In NPG nanoparticles, however, the Disk LSPR mode dominates the extinction spectrum and is blueshifted during prolonged dealloying. Since the thickness and disk diameter at various dealloying was nearly identical as mentioned above, the observed blueshift was primarily due to pore coarsening, further supporting the presence of plasmonic coupling between the Disk LSPR and NPG LSPR modes besides apparent spectra overlap.

In our previous work,[11] we discovered that the plasmonic coupling between the in-plane Disk LSPR and NPG LSPR generated high density hot-spots concentrated near the pores around the circumference of NPG disk. It is well known that the plasmonic extinction band redshifts as inter-particle coupling increases when individual nanoparticles aggregate.[25–29] Conversely, blueshift is observed due to the decreased coupling when the interparticle distance increases. Therefore, for NPG nanoparticles, the blueshift can also be understood as a decrease of the plasmonic coupling between the in-plane Disk LSPR and NPG LSPR caused by the increased pore and ligament size. According to Chen and coworkers' simulation,[30] the EM field enhancement of NPG thin films decays with increasing pore and ligament size which indicates that the small pores accompanied with small ligaments provide the stronger LSPR than large ones. Examining as-dealloyed NPG nanoparticles (Fig. 1), both pore and ligament size gradually increased with dealloying time, and the largest pore and ligament at 270 s were ~4 and 7 nm larger than those at 30 s, respectively. Hence, NPG nanoparticles at 30 s with the smallest pore and ligament generate the strongest LSPR (*e.g.*, NPG LSPR) to couple with Disk LSPR, its plasmonic extinction band exhibits the largest redshift. The band blueshifted as the coupling decreases because of the decreased LSPR of the larger pore and ligament (Fig. 2b). To our knowledge, this unique interpretation of interplay between external and internal LSPR modes has never been reported before.

To further investigate the Au atomic composition effect on the plasmonic extinction band, we used a different alloy target ($Ag_{70}Au_{30}$) and followed the same experimental protocols. Fig. 3 shows SEM images of as-dealloyed NPG nanoparticles and the extinction band from 30 to 270 s. The corresponding average diameters at 30 and 270 s were ~319 ± 9 nm. For 30 s (Fig. 3a), the average pore size was about 7.8 nm, and the average ligament size was about 10.5 nm, both smaller compared to those obtained from the $Ag_{82.5}Au_{17.5}$ target at 30 s (Fig. 1a). Apparently, the alloy composition with the higher percentage of Au experienced less Ag removal that caused the decrease of the pore and ligament size, agreeing with previous reports on NPG films by Gupta and Lu.[24,31] This has also been confirmed by XPS analysis as shown in Fig. S2.† The Ag atomic composition for the $Ag_{70}Au_{30}$ starting alloy decreased from 70% to 27.4% within 30 s as compared to from 82.5% to 23.8% for the $Ag_{82.5}Au_{17.5}$ starting alloy. As the dealloying time was increased to 270 s (Fig. 3b), the average size of pores and ligaments increased to ~12 and ~20.8 nm, respectively. Since morphology can be significantly affected by the higher Au atomic composition, it is interesting to investigate their plasmonic properties. As shown in Fig. 3c, a broad extinction band appears in the range from 900 to 1000 nm with the maximum at 920 nm after dealloyed for 30 s. When the dealloying time gradually increased, the

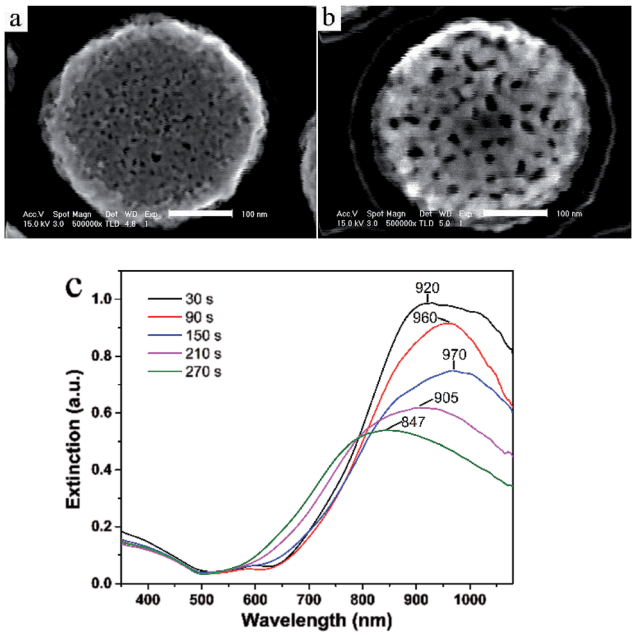

Fig. 3 SEM images and extinction spectra of ~300 nm diameter NPG disk made from $Ag_{70}Au_{30}$ alloy: (a) and (b) are the SEM images of NPG disk at 30 s and 270 s, and (c) extinction spectra *versus* dealloying time. SEM scale bar: 100 nm.

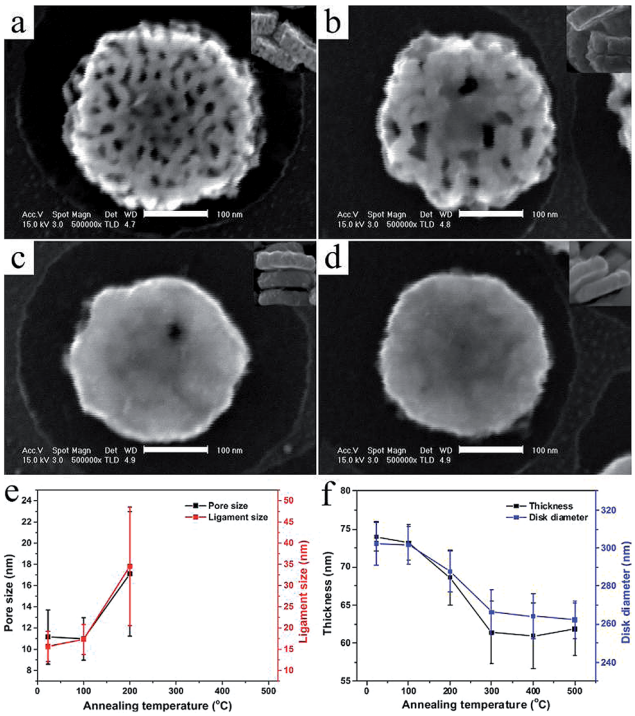

Fig. 4 SEM images of NPG nanoparticles after different annealing temperature: (a) 100, (b) 200, (c) 300, and (d) 400 °C. The insets show thickness. (e) the changes of pore and ligament size *versus* annealing temperature, and (f) is the thickness and NPG disk diameter *versus* annealing temperature. SEM scale bar: 100 nm.

maximum band first redshifted to 970 nm at 150 s and then began to blueshift with further dealloying. At 270 s, the band blueshifted to 847 nm which is lower than that of as-dealloyed NPG nanoparticles from $Ag_{82.5}Au_{17.5}$ atomic composition. Intuitively, the higher Au atomic composition could induce NPG nanoparticle morphological changes that results in significant plasmonic shift. Thus, different alloy atomic compositions offers an alternative way to tune the plasmon resonance of NPG nanoparticles.

Thermal annealing dependent blueshift

Post-dealloying thermal annealing is known to provide an alternative way to modify pore and ligament structures in NPG thin films, owing to nanostructural coarsening.[7–9,32] To further explore morphology-dependent plasmonic resonance, we annealed NPG nanoparticles dealloyed at 30 s with 300 nm diameter and 74 nm thickness at 100, 200, 300, 400, and 500 °C for 30 min in the protection of Argon gas, with SEM images shown in Fig. 4a–d, respectively. The insets allow the estimate for disk thickness. Fig. 4e and f show the statistical analysis of pore size, ligament size, thickness and diameter *versus* annealing temperature. The morphology exhibits moderate changes in the ligament size and thickness as the temperature increased from 23 to 100 °C (Fig S3a† and 4a). At 200 °C, the pore and ligament size significantly increased from 11 to 17 nm (Fig. 4b).

In addition, their thickness and diameter decreased by ~7 and 15 nm, respectively. As shown in Fig. 4c, d and S3c,† the pore coalescence led to smoother surfaces lacking of characteristic nonporous structures when the temperature was further increased to 300, 400, and 500 °C. Moreover, there was negligible change in both the thickness and diameter from 300 to 500 °C. The mechanism of thermal coarsening was well understood as a two-staged process through both theoretical simulation and experimental study to reveal the stability and morphological evolution of nanoporous materials in previous reports.[9,33,34] The first stage involves surface diffusion of Au atoms, which occurs at relatively low temperature. The second stage involves volume diffusion and ligament collapse, which occur at relatively high temperatures. Our NPG nanoparticles exhibited slight changes in the pore, ligament and diameter sizes when annealed at 100 °C, while the ligaments significantly collapsed onto one another at higher temperature (200–500 °C), resulting in pore closure and significant decrease in diameter and thickness. XPS, a technique sensitive to surface composition, revealed that the surface composition of Au increases from 76.2% to 81.6% after thermal annealing to further confirm the coarsening evolution of nanoporous structures. These observations and measurement results agree well with the current understanding of thermal coarsening in NPG.

Fig. 5a shows the extinction spectra of NPG nanoparticles after annealing at different temperature. The in-plane Disk LSPR at 988 nm blueshifted for around 23, 150, and 250 nm after annealing at 100, 200, and 300 °C, respectively, agreeing with the trends of morphological changes observed in the SEM images. Further increasing the annealing temperature up to 500 °C led to less change because pores started to coalesce and close

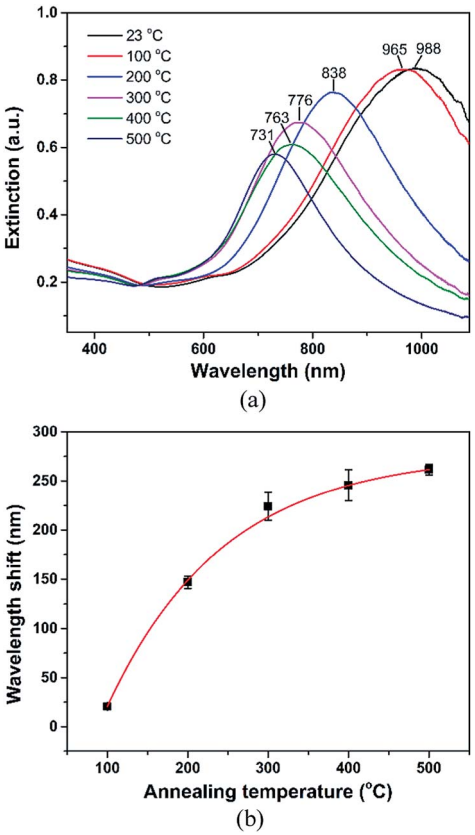

Fig. 5 Extinction spectra of 300 nm as-dealloyed NPG nanoparticles from $Ag_{82.5}Au_{17.5}$ alloy at 30 s before and after annealing: (a) extinction bands after annealing at different temperatures and (b) the wavelength blueshift as a function of annealing temperatures.

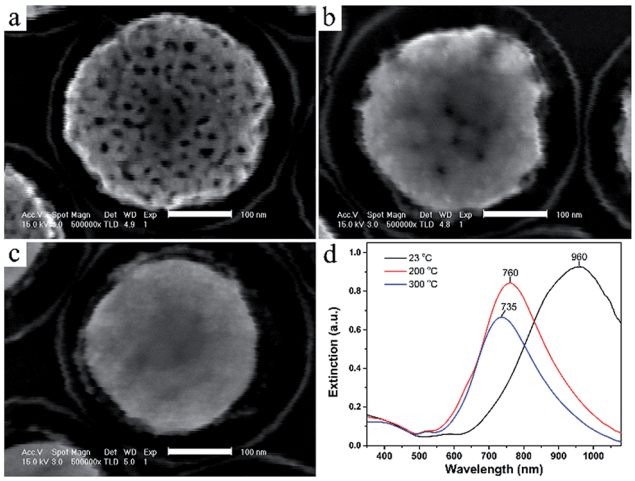

Fig. 6 SEM images of ~300 nm NPG nanoparticles dealloyed at 90 s from $Ag_{70}Au_{30}$ alloy at (a) 23 °C, (b) 200 °C and (c) 300 °C. (d) Extinction spectra at corresponding temperatures. SEM scale bar: 100 nm.

up and the external dimensions stopped to change at around 300 °C. Apparently, the rapid morphological evolution of NPG nanoparticles between 100 and 300 °C has significant impact on its plasmonic resonance. The blueshift can also be understood from the evolution of disk diameter by comparing with an Au disk without pores. It is well understood that the in-plane resonance band blueshifts in Au nanoparticles as the diameter decreases.[35,36]

As shown in Fig. 4f, the NPG disk diameter decreased 14 nm after annealing at 200 °C, and then it further decreased 21 nm at 300 °C. After the pores closed up, the non-porous nanoparticles exhibited good stability at the higher temperature above 300 °C. The diameter only further decreased 4 nm even at the highest temperature (500 °C), while the thickness was almost the same. Correspondingly, the Disk LSPR further slightly blueshifted to 260 nm. The most significantly incremental blueshift (~70 nm) happened after annealing at 200 °C, and then less incremental shift was observed at higher temperature. Thermal annealing of as-dealloyed NPG nanoparticles from $Ag_{70}Au_{30}$ alloy was also investigated to understand composition effect on morphological changes, as well as plasmonic resonance. Fig. 6a–c show the corresponding SEM images after annealing at 23, 200 and 300 °C, respectively. We observed the porous nanostructures significantly changed at 200 °C, where the pores closed up and the disk became non-porous. The average diameter decreased ~26 nm. At 300 °C, the average diameter of NPG nanoparticles further decreased ~12 nm and the surface became smoother after pore coalescence. The surface composition of Au also increased ~3% after thermal annealing as determined by XPS. As shown in Fig. 6d, the in-plane Disk LSPR at 960 nm blueshifted to 760 nm after annealed at 200 °C. The wavelength shift was up to ~200 nm, much larger than that of from the $Ag_{82.5}Au_{17.5}$ (~127 nm) alloy target. However, the plasmonic resonance slightly changed after the temperature increased to 300 °C. The SEM images (Fig. 6a–c) further support that the large shift was induced by the significant changes of NPG nanoparticle nanostructures such as the disk diameter and pore size.

According to previous reports for semi-infinite NPG films,[8–10] by using Au atomic compositions ranging from 25% to 35%, the structural coarsening at 200 °C induced substantial morphology changes in increased pore and ligament size. Their pore and ligament size continuously grows larger up to a few hundred nanometers when they were further annealed at higher temperature. However, NPG nanoparticles obtained from both Au atomic compositions 17.5% and 30% exhibited completely different morphology changes compared to NPG films. Thus, the differences in the morphological evolution between NPG films and NPG nanoparticles should primarily originate from their architecturally distinct features. Heuristically, individual NPG nanoparticles lack the longer-ranged structural network organization as seen in the semi-infinite NPG films, leading to a free-to-deform boundary condition around the disk circumference, thus more prominent Au diffusion at elevated temperature.

Surface-enhanced Raman scattering (SERS) characterization

Raman scattering is known to provide molecular fingerprints and can be greatly enhanced by gold or silver

nanostructures.[12,37] To explore the tunable plasmonic properties for SERS application, we take NPG nanoparticles obtained from $Ag_{82.5}Au_{17.5}$ alloy as an example to measure Raman spectra of benenzethiol (BT) molecules. Fig. 7a and b show BT spectra on NPG nanoparticles at different dealloyed time and thermal annealing temperatures, respectively. As the dealloyed time increased, SERS intensity gradually increased (Fig. 7c). However, SERS intensity significantly dropped after thermally treated at 200 °C (Fig. 7d). The enhancement factor (EF) estimated for 30 and 270 s dealloying time was 1.64×10^6 and 3.31×10^6, respectively, while it decreased to 3.97×10^4 at 200 °C. The increased SERS EF for longer dealloying time could be understood based on the electromagnetic theory, where the maximum SERS enhancement can be achieved when the LSPR peak matches the average of the laser excitation and Raman wavelengths.[38,39] Here, the average wavelength is ~821 nm with 785 nm excitation wavelength and 857 nm Raman wavelength (1077 cm^{-1}). Therefore, when the tunable LSPR peak of NPG nanoparticles moved closer to the average wavelength, the resulting SERS enhancement became larger.

Interestingly, when NPG nanoparticles were thermally treated with LSPR peak tuning from 988 to 838 nm, the SERS enhancement significantly decreased instead of the increase. Apparently, there are other important factors dominating the enhancement rather than the tunable LSPR. According to Qian *et al.*, the nanoporous structure and surface roughness are considered to be important features for SERS enhancement of nanoporous gold materials, where higher enhancement was observed in NPG films with smaller pore size and rougher surface.[8] High temperature annealing causing the pore size enlargement and surface smoothening led to low SERS enhancement. As shown in SEM images (Fig. 4), the NPG disk surface became smoother accompanied with vanishing pores upon thermal annealing. Therefore, these two factors correspond to the drop of SERS enhancement. This observation is consistent with Qian's work.

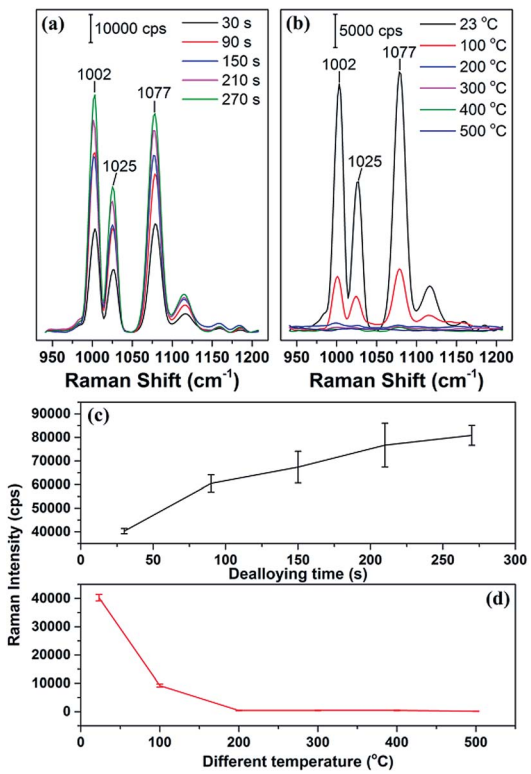

Fig. 7 Surface-enhanced Raman spectra of benzenethiol ranging from 930 to 1210 cm^{-1} on NPG nanoparticles obtained from $Ag_{82.5}Au_{17.5}$ alloy: (a) different dealloying time and (b) different annealing temperatures for NPG nanoparticles obtained after 30 s dealloying; (c) and (d) are the change trends of intensity of the SERS band at 1077 cm^{-1} corresponding to different dealloying time and temperatures, respectively.

Conclusions

In summary, we studied morphology-dependent plasmonic extinction of monolithic NPG nanoparticles by structural evolution induced separately by timed dealloying in concentrated nitric acid and post-dealloying thermal annealing, and varying the Au atomic compositions. The plasmonic properties depend on the internal parameters such as pore and ligament size, as well as external parameters such as the disk thickness and diameter. The extinction bands are tuned within a wide spectral region from 730 to 980 nm upon the changes of pore, ligament and diameter sizes. The tunable spectral region is much larger than that of the semi-infinite NPG films from 550 to 600 nm. In addition, the monolithic NPG nanoparticles provide external shape parameters such as disk diameter to monitor the plasmonic resonance. It exhibits a great potential in the applications of SERS and plasmonic sensing. The intricate coupling between the Disk and NPG LSPR modes has been further elucidated by our experimental results.

Acknowledgements

W.C.S. acknowledges the National Science Foundation (NSF) CAREER Award (CBET-1151154), National Aeronautics and Space Administration (NASA) Early Career Faculty Grant (NNX12AQ44G) and a grant from Gulf of Mexico Research Initiative (GoMRI-030).

Notes and references

1 Y. Ding and M. Chen, *MRS Bull.*, 2009, **34**, 569–576.
2 F. Yu, S. Ahl, A.-M. Caminade, J.-P. Majoral, W. Knoll and J. Erlebacher, *Anal. Chem.*, 2006, **78**, 7346–7350.
3 X. Lang, L. Qian, P. Guan, J. Zi and M. Chen, *Appl. Phys. Lett.*, 2011, **98**, 093701–093703.
4 K. A. Willets and R. P. Van Duyne, *Annu. Rev. Phys. Chem.*, 2007, **58**, 267–297.
5 X. Lang and M. Chen, in *Nanoporous Gold: From an Ancient Technology to a High-Tech Material*, ed. Arne Wittstock *etc.*, Royal Society of Chemistry, 2012, ch. 6.
6 Y. Fu, J. Zhang, K. Nowaczyk and J. R. Lakowicz, *Chem. Commun.*, 2013, **49**, 10874–10876.
7 S. O. Kucheyev, J. R. Hayes, J. Biener, T. Huser, C. E. Talley and A. V. Hamza, *Appl. Phys. Lett.*, 2006, **89**, 053102–053103.

8 L. Qian, X. Yan, T. Fujita, A. Inoue and M. Chen, *Appl. Phys. Lett.*, 2007, **90**, 153120–153123.
9 J. Wang, R. Xia, J. Zhu, Y. Ding, X. Zhang and Y. Chen, *J. Mater. Sci.*, 2012, **47**, 5013–5018.
10 R. N. Viswanath, V. A. Chirayath, R. Rajaraman, G. Amarendra and C. S. Sundar, *Appl. Phys. Lett.*, 2013, **102**, 253101–253103.
11 F. Zhao, J. Zeng, M. M. P. Arnob, P. Sun, J. Qi, P. Motwani, M. Gheewala, C.-H. Li, A. Paterson, U. Strych, B. Raja, T. R. Lee, R. C. Willson, J. C. Wolfe and W.-C. Shih, *Nanoscale*, 2014, **6**, 8199–8207.
12 J. Qi, P. Motwani, M. Gheewala, C. Brennan, J. C. Wolfe and W.-C. Shih, *Nanoscale*, 2013, **5**, 4105–4109.
13 G. M. Santos, F. Zhao, J. Zeng and W.-C. Shih, *Nanoscale*, 2014, **6**, 5718–5724.
14 J. R. Cole, N. A. Mirin, M. W. Knight, G. P. Goodrich and N. J. Halas, *J. Phys. Chem. C*, 2009, **113**, 12090–12094.
15 Q. Tian, F. Jiang, R. Zou, Q. Liu, Z. Chen, M. Zhu, S. Yang, J. Wang, J. Wang and J. Hu, *ACS Nano*, 2011, **5**, 9761–9771.
16 M. Li, J. Lu, J. Qi, F. Zhao, J. Zeng, J. C.-C. Yu and W.-C. Shih, *J. Biomed. Opt.*, 2014, **19**, 050501.
17 M. Li, F. Zhao, J. Zeng, J. Qi, J. Lu and W.-C. Shih, *J. Biomed. Opt.*, 2014, **19**, 111611.
18 J. Rybczynski, U. Ebels and M. Giersig, *Colloids Surf., A*, 2003, **219**, 1–6.
19 W.-d. Ruan, Z.-c. LÜ, N. Ji, C.-x. Wang, B. Zhao and J.-h. Zhang, *Chem. Res. Chin. Univ.*, 2007, **23**, 712–714.
20 J. Qi and W. -C. Shih, *Appl. Opt.*, 2014, **53**, 2881–2885.
21 J. Erlebacher, M. J. Aziz, A. Karma, N. Dimitrov and K. Sieradzki, *Nature*, 2001, **410**, 450–453.
22 Y. Ding, Y. J. Kim and J. Erlebacher, *Adv. Mater.*, 2004, **16**, 1897–1900.
23 J. Erlebacher, R. C. Newman and K. Sieradzki, in *Nanoporous Gold: From an Ancient Technology to a High-Tech Material*, ed. Arne Wittstock *etc.*, Royal Society of Chemistry, 2012, ch. 2.
24 G. Gupta, J. Thorp, N. Mara, A. Dattelbaum, A. Misra and S. Picraux, *J. Appl. Phys.*, 2012, **112**, 094320–094327.
25 W. Rechberger, A. Hohenau, A. Leitner, J. Krenn, B. Lamprecht and F. Aussenegg, *Opt. Commun.*, 2003, **220**, 137–141.
26 I. Romero, J. Aizpurua, G. W. Bryant and F. J. García De Abajo, *Opt. Express*, 2006, **14**, 9988–9999.
27 J. B. Lassiter, J. Aizpurua, L. I. Hernandez, D. W. Brandl, I. Romero, S. Lal, J. H. Hafner, P. Nordlander and N. J. Halas, *Nano Lett.*, 2008, **8**, 1212–1218.
28 F. J. García de Abajo, *J. Phys. Chem. C*, 2008, **112**, 17983–17987.
29 N. J. Halas, S. Lal, W.-S. Chang, S. Link and P. Nordlander, *Chem. Rev.*, 2011, **111**, 3913–3961.
30 X. Y. Lang, P. F. Guan, L. Zhang, T. Fujita and M. W. Chen, *J. Phys. Chem. C*, 2009, **113**, 10956–10961.
31 X. Lu, T. Balk, R. Spolenak and E. Arzt, *Thin Solid Films*, 2007, **515**, 7122–7126.
32 E. Seker, J. T. Gaskins, H. Bart-Smith, J. Zhu, M. L. Reed, G. Zangari, R. Kelly and M. R. Begley, *Acta Mater.*, 2007, **55**, 4593–4602.
33 K. Kolluri and M. J. Demkowicz, *Acta Mater.*, 2011, **59**, 7645–7653.
34 M. P. Klein, B. W. Jacobs, M. D. Ong, S. J. Fares, D. B. Robinson, V. Stavila, G. J. Wagner and I. Arslan, *J. Am. Chem. Soc.*, 2011, **133**, 9144–9147.
35 I. Zorić, M. Zäch, B. Kasemo and C. Langhammer, *ACS Nano*, 2011, **5**, 2535–2546.
36 Y.-C. Chang, H.-C. Chung, S.-C. Lu and T.-F. Guo, *Nanotechnology*, 2013, **24**, 095302.
37 W.-C. Shih, K. Bechtel and M. S. Feld, in *Noninvasive glucose sensing with Raman spectroscopy*, ed. D. D. Cunningham and J. A. Stenken, John Wiley & Sons, 2009, ch. 2.
38 N. Félidj, J. Aubard, G. Lévi, J. R. Krenn, M. Salerno, G. Schider, B. Lamprecht, A. Leitner and F. R. Aussenegg, *Phys. Rev. B: Condens. Matter Mater. Phys.*, 2002, **65**, 075419.
39 E. C. L. Ru and P. G. Etchegoin, *Principles of Surface-Enhanced Raman Spectroscopy and related plasmonic effects*, Elsevier Inc, 1st edn, 2009.

